46th AIAA Aerospace Sciences Meeting and Exhibit
7 - 10 January 2008, Reno, Nevada

AIAA 2008-145

Aerodynamic-Structural Design Studies of Low-Sweep Transonic Wings

Antony Jameson*
Department of Aeronautics and Astronautics
Stanford University, Stanford, CA 94305-3030

John C. Vassberg†
Hydro-Aero Consulting Group
Long Beach, CA 90803

Sriram Shankaran‡
Consultant
Schenectady, NY

Abstract

The work presented herein explores the possibility of extending some commonly accepted limits related to the general layout of an efficient transonic wing. Specifically, the Mach-Sweep-Thickness relationships are revisited at a cursory level. High-fidelity aerodynamic and aerodynamic-structural optimizations are performed on a set of wings constructed by a parametric variation on wing sweep. These study wings are derived from a baseline wing representative of current aircraft design practices. Initial results show that it may be possible to significantly reduce wing sweep without incurring either aerodynamic or structural penalties, especially for $M \leq 0.8$ aircraft designs. Although more work is required to better quantify the magnitude of the potential improvements possible. Nonetheless, with existing aerodynamic and aerodynamic-structural optimization software, the possibility of enhancing the current knowledge base of wing planform layout is now within grasp.

Background

The current generation of civilian transport aircraft are typically designed with a moderately high swept wing. However, the planform layout of these wings were substantially influenced by historical design charts developed decades ago. These design charts were derived and updated from wind-tunnel and flight data collected over the years; they include shifts due to technology levels, such as that introduced by supercritical airfoil sections. Most of the wing geometries that form the basis of these data were designed using cut-and-try methods and augmented with parametric variations of sweep, thickness, lifting condition, and freestream Mach number. More importantly, this knowledge base was predominately developed before the advent of modern high-fidelity simulation capabilities and multi-disciplinary optimization tools. With rapid advances in the numerical simulation of high Reynolds-number flows and efficient shape optimization techniques, it is now feasible to revisit the general layout drivers of transonic wing planforms for the benefit of future commerical transport aircraft. Specifically, it may be currently possible to extend the accepted bounding limit of the Mach-Sweep-Thickness ($M\Lambda T$) relationships. Recent results from an aerodynamic shape optimization of a low-sweep wing of a modern transonic transport have shown that it is possible to delay the drag rise of this wing to beyond a Mach number of 0.8.

Driven by escalating fuel costs as well as by environmental concerns, it is highly likely that future aircraft designs will be directed to deliver improved performance with significantly reduced fuel burn per passenger mile, even if it incurs a modest increase in mission block time. For example, a *sweet spot* in the aircraft design space may exist near $M = 0.8$, where an unducted-fan engine could be utilized - thus yielding large reductions in specific fuel consumption. If it is possible to develop an efficient low-sweep wing capable of $M = 0.8$ cruise, then other synergies such as reductions in manufacturing costs could also be exploited.

In this work, we systematically study the feasibility of designing wings with reduced sweep without incurring aerodynamic or structural performance penalities. Pure aerodynamic optimizations of transonic wings with varying sweeps ($5^\circ \leq \Lambda \leq 35^\circ$) show that the $M\Lambda T$ design space may be relatively flat with respect to ML/D, thus

*Thomas V. Jones Professor of Engineering, Fellow AIAA
†Boeing Technical Fellow, Associate Fellow AIAA
‡Technology Philanthropist

yielding higher range factors at reduced cruise Mach numbers. These aerodynamically optimized configurations were further studied using an aerodynamic-structural optimization package along with planform variations. The aerodynamic-structural optimizations reveal that the $M\Lambda T$ design space remains relatively flat with respect to ML/D and Operator Empty Weight (OEW), thus confirming the conclusion that wings with low sweep can be effectively used as an alternative to current higher swept-back configurations.

Approach

The approach taken in this study is organized into two phases. In the first phase, pure aerodynamic optimizations were conducted on a parametric variation of wing sweep, while holding structural beam properties (lengths and depths) of the exposed wing constant. In the second phase, the aerodynamically optimal wings from the initial phase were re-optimized with a coupled aerodynamic-structural method.

Geometry Set-Up

To establish a consistant set of seed geometries of varying sweep, a baseline wing/body configuration typical of current aircraft-design practices was utilized. This baseline wing/body configuration was developed to cruise efficiently at a Mach number of $M = 0.85$ and a lift coefficient of $C_L = 0.5$; its planform (with defining stations) is depicted in Figure 1. Figure 2 shows its nondimensional thickness $max\text{-}T/C$ (left) and corresponding absolute thickness $max\text{-}T$ in $inches$ (right). Reference quantities are:

$$Sref = 4,000\ ft^2,\ b = 192.8\ ft,\ Cref = 275.8\ in,\ AR = 9.29,\ \lambda = 0.275,$$

where $Sref$ is the wing reference area, b is the wing span, $Cref$ is the wing reference chord, $AR = b^2/Sref$ is the wing aspect ratio, and λ is the taper ratio of the trap wing. The trap wing of this layout has a quarter-chord sweep of $\Lambda = 35°$. Its side-of-body (SOB) is located at 10% semispan, which is at a wing butt line (WBL) location of $115.7\ in$. Its average nondimensional thickness is about 11.5%.

In order to generate the additional seed wings needed for this investigation, the quarter-chord line of the baseline wing was rotated about its SOB location. Each defining airfoil section was simply translated by the movement of its quarter-chord location per the aforementioned rotation. Hence, the absolute dimensions and orientation of each defining airfoil station were not altered relative to the baseline wing. The final modification in establishing the seed wings was to retwist and re-rig the wings to provide a similar spanload distribution as that of the baseline wing at a similar fuselage angle-of-attack. Note that these transformations generate seed wings which retain the sturctural properties of the baseline wing's beam length and depth. On the other hand, the aerodynamic span, true wing area, and fuel volume all increase accordingly with a reduction in wing sweep. Table 1 gives the variation of wing span as a function of sweep angle. While the true wing area varies as a result of this transformation, in this study the wing reference area was held constant and equivalent to that of the baseline wing. Holding wing reference area constant simplifies a drag build-up (described later) representative of a complete aircraft.

The purpose of setting up the reduced-sweep wings in the above manner was motivated by the desire to have the ability to perform pure aerodynamic optimizations, while essentially not impacting wing structural weight. The second phase of our study has verified this underlying assumption.

There are a couple of other items to note. The resulting yehudi regions inboard of the planform break are likely not laid out as they naturally would be in an actual aircraft design. Further, no attempt was made to resize these study wings per real aircraft design considerations. Both of these elements introduce non-optimal characteristics in the planform layout of the study wings, especially for those with sweep deviating most from that of the baseline. In this respect, the findings herein for the lowest-sweep wings may be overly conservative.

Pure Aerodynamic Optimization

The primary goal of the present work was to develop evidence that may challenge the conventional wisdom on what is possible in the $M\Lambda T$ design space for efficient transonic cruise. In order to accomplish this in a rigorous manner, one would have to comprehensively survey the $Mach\text{-}C_L$ space for each of the seven sweep angles under study. This would require on the order of 200 aerodynamic shape optimizations to be performed. Since this level of effort was far beyond the scope of this initial investigation, instead we surveyed the $Mach\text{-}C_L$ space for the $\Lambda = 10°$ wing to determine reasonable design conditions for this case. We made educated judgements to estimate what flow conditions should be used for the remaining sweep angles. Single-point aerodynamic optimizaitons were conducted for the remaining sweep angles, starting with each of the seed wings, at their corresponding design conditions. To be consistant with this study, the baseline $\Lambda = 35°$ wing was also re-optimized at its single-point design condition. The shape modifications were constrained to maintain thickness everywhere on the wing, relative to the starting geometries. However, the spanload distribution was allowed to fall out from the

optimizations. Note that the aerodynamically optimum spanload for a transonic wing is not necessarily elliptic; e.g., shock and induced drags are traded accordingly. (As it turned out, the spanload distributions of the optimal wings tended to closely match each other without a constraint being applied.)

These aerodynamic optimizations yielded estimates of the minimum drag level possible for each of the wings; simulated as a wing/body configuration. To estimate an absolute drag level for the full configuration aircraft, the wing drag (C_D) was augmented with an estimate of the drag for the residual aircraft (fuselage, pylons, nacelles, empennage, excressences, and in static trim). This residual drag was taken as $C_{D.res} = 140$ *counts* relative to the fixed reference area used for all of the study wings; total aircraft drag is then $C_{D.tot} = C_D + C_{D.res}$. Based on this rudimentary drag build-up, the quantified metrics of ML/D and $\sqrt{M}L/D$ are representative of the aircraft in flight. Here, ML/D is a measure of aerodynamic performance, while $\sqrt{M}L/D$ is approximately proportional to range factor. According to the Breguet range equation

$$R = \frac{ML}{D}\frac{a}{SFC}ln\frac{W_1}{W_2},$$

the range efficiency may be estimated by $[(M/SFC)(L/D)]$. Here, a is the speed of sound, SFC is the specific fuel consumption, and W_1 and W_2 are the take-off and landing weights, respectively. The SFC of a turbofan engine typically increases with Mach number at a rate which is fairly well approximated by a linear variation with a slope around 0.5. Accordingly $\sqrt{M}L/D$ may be regarded as a useful indicator of the range factor.

Aerodynamic-Structural Optimization

The resulting geometries of the pure aerodynamic optimizations were studied further with a coupled aerodynamic-structural optimization methodology, which explicitly includes the trade-off between aerodynamic drag and wing structural weight. This explicit tie between aerodynamics and structural weight, allowed these optimizations the ability to appropriately vary wing thickness, span, and sweep. However, we note that the FEM-based process utilized herein is not nearly as rigorous as those employed within a real aircraft design environment, which include numerous off-design and flutter conditions scattered throughout the fight envelope; any one of which may size the structure. Specifically, our aerodynamic-structural optimizations were all conducted at single-point cruise conditions, and incorporate a surrogate metric of material stress. Here, the allowable material stress distribution is defined by that of the baseline $\Lambda = 35^\circ$ wing. This allowable stress distribution is utilized during the inner-loop structural optimizations to resize the wing skin thicknesses, and therefore provide estimates for the wing structural weights.

In order to conduct a single-objective aerodynamic-structural optimization, a cost function is developed which blends the coefficients of drag (C_D) and weight (C_W) together in such a manner as to maximize range, while holding Mach number and fuel volume constant.

The following two sections provide an overview of the mathematical developments of both the pure aerodynamic optimization and the aerodynamic-sturctural optimization methodologies.

Aerodynamic Optimization Methodology

The shape optimization methodology used in this work is based on the theory of optimal control of systems governed by partial differential equations, where the control is by varying the shape of the boundary.[1–5] The gradient of a cost function, in this case the drag coefficient with respect to the shape, is obtained by solving the adjoint equation. An outline of the procedure is as follows. Suppose that the cost function are functions of the state variables, w, and the control variables, which may be represented by the function, $\mathcal{F}$, say. Then

$$I = I(w, \mathcal{F}),$$

and a change in $\mathcal{F}$ results in a change

$$\delta I = \frac{\partial I^T}{\partial w}\delta w + \frac{\partial I^T}{\partial \mathcal{F}}\delta \mathcal{F}, \tag{1}$$

in the cost function. Using control theory, the governing equations for the state variables are introduced as a constraint in such a way that the final expression for the gradient does not require re-evaluation of the state. In order to achieve this, δw must be eliminated from equation 1. Suppose that the governing equation R which expresses the dependence of w and $\mathcal{F}$ within the domain D can be written as

$$R(w, \mathcal{F}) = 0 \tag{2}$$

Then δw is determined from the equation

$$\delta R = \left[\frac{\partial R}{\partial w}\right] \delta w + \left[\frac{\partial R}{\partial \mathcal{F}}\right] \delta \mathcal{F} = 0 \tag{3}$$

Next, introducing a Lagrange Multiplier ψ, we have

$$\delta I = \frac{\partial I^T}{\partial w}\delta w + \frac{\partial I^T}{\partial \mathcal{F}}\delta \mathcal{F} - \psi^T \left(\left[\frac{\partial R}{\partial w}\right] \delta w + \left[\frac{\partial R}{\partial \mathcal{F}}\right] \delta \mathcal{F} \right)$$

$$\delta I = \left(\frac{\partial I^T}{\partial w} - \psi^T \left[\frac{\partial R}{\partial w}\right] \right) \delta w + \left(\frac{\partial I^T}{\partial \mathcal{F}} - \psi^T \left[\frac{\partial R}{\partial \mathcal{F}}\right] \right) \delta \mathcal{F}$$

Choosing ψ to satisfy the adjoint equation

$$\left[\frac{\partial R}{\partial w}\right]^T \psi = \frac{\partial I}{\partial w} \tag{4}$$

the first term is eliminated and we find that

$$\delta I = \mathcal{G} \delta \mathcal{F} \tag{5}$$

where

$$\mathcal{G} = \frac{\partial I^T}{\partial \mathcal{F}} - \psi^T \left[\frac{\partial R}{\partial \mathcal{F}}\right] \tag{6}$$

This process allows for elimination of the terms that depend on the flow solution with the result that the gradient with respect with an arbitrary number of design variables can be determined without the need for additional flow field evaluations.

After taking a step in the negative gradient direction, the gradient is recalculated and the process repeated to follow the path of steepest descent until a minimum is reached. In order to avoid violating constraints, such as the minimum acceptable wing thickness, the gradient can be projected into an allowable subspace within which the constraints are satisfied. In this way one can devise procedures which must necessarily converge at least to a local minimum and which can be accelerated by the use of more sophisticated descent methods such as conjugate gradient or quasi-Newton algorithms. There is a possibility of more than one local minimum, but in any case this method will lead to an improvement over the original design.

The derivation of the adjoint equation and boundary conditions for optimization using the Reynolds averaged Navier-Stokes equations is presented in detail by Jameson.[4]

A key issue for successful implementation of the continuous adjoint method is the choice of an appropriate inner product for the definition of the gradient. It turns out that there is an enormous benefit from the use of a modified Sobolev gradient, which enables the generation of a sequence of smooth shapes.[6,7] This can be illustrated by considering the simplest case of a problem in calculus of variations.

Choose $y(x)$ to minimize

$$I = \int_a^b F(y, y')dx$$

with fixed end points $y(a)$ and $y(b)$. Under a variation $\delta y(x)$,

$$\begin{aligned} \delta I &= \int_a^b \left(\frac{\partial F}{\partial y}\delta y + \frac{\partial F}{\partial y'}\delta y' \right) dx \\ &= \int_a^b \left(\frac{\partial F}{\partial y} - \frac{d}{dx}\frac{\partial F}{\partial y'} \right) \delta y dx \end{aligned}$$

Thus defining the gradient as

$$g = \frac{\partial F}{\partial y} - \frac{d}{dx}\frac{\partial F}{\partial y'}$$

and the inner product as

$$(u, v) = \int_a^b uvdx$$

we find that

$$\delta I = (g, \delta y)$$

Then if we set

$$\delta y = -\lambda g, \qquad \lambda > 0$$

we obtain a improvement

$$\delta I = -\lambda(g, g) \leq 0$$

unless $g = 0$, the necessary condition for a minimum. Note that g is a function of $y, y^{'}, y^{''}$,

$$g = g(y, y^{'}, y^{''})$$

In the case of the Brachistrone problem, for example

$$g = -\frac{1 + y^{'2} + 2yy^{''}}{2\left(y(1 + y'^2)\right)^{3/2}}$$

Now each step

$$y^{n+1} = y^n - \lambda^n g^n$$

reduces the smoothness of y by two classes. Thus the computed trajectory becomes less and less smooth, leading to instability.

In order to prevent this we can introduce a modified Sobolev inner product

$$\langle u, v\rangle = \int (uv + \epsilon u^{'} v^{'})dx$$

where ϵ is a parameter that controls the weight of the derivatives. If we define a gradient $\overline{g}$ such that

$$\delta I = \langle \overline{g}, \delta y\rangle$$

Then we have

$$\begin{aligned} \delta I &= \int (\overline{g}\delta y + \epsilon \overline{g}^{'} \delta y^{'})dx \\ &= \int (\overline{g} - \frac{\partial}{\partial x}\epsilon\frac{\partial \overline{g}}{\partial x})\delta y dx \\ &= (g, \delta y) \end{aligned}$$

where

$$\overline{g} - \frac{\partial}{\partial x}\epsilon\frac{\partial \overline{g}}{\partial x} = g$$

and $\overline{g} = 0$at the end points. Thus $\overline{g}$ is obtained from g by a smoothing equation.

Now the step

$$y^{n+1} = y^n - \lambda^n \overline{g}^n$$

gives an improvement

$$\delta I = -\lambda^n \langle \overline{g}^n, \overline{g}^n\rangle$$

but y^{n+1} has the same smoothness as y^n, resulting in a stable process.

In applying control theory for aerodynamic shape optimization, the use of a Sobolev gradient is equally important for the preservation of the smoothness class of the redesigned surface, and we have employed it to obtain all the results in this study. With this approach there is no need to parametrize the geometry. Instead it is treated as a free surface, with shape modifications controlled by movement of the surface mesh points.[8]

Outline of the Design Process

The design procedure can be summarized as follows.

1. Solve the flow equations for ρ, u_1, u_2, u_3, p.
2. Solve the adjoint equations for ψ subject to appropriate boundary conditions.
3. Evaluate $\mathcal{G}$ and calculate the corresponding Sobolev gradient $\bar{\mathcal{G}}$.
4. Project $\bar{\mathcal{G}}$ into an allowable subspace that satisfies any geometric constraints.
5. Update the shape based on the direction of steepest descent.
6. Return to 1 until convergence is reached.

This aerodynamic shape optimization has been applied extensively by the authors over the past 15 years with much success on a wide variety of configurations including a Reno Race Plane and a Mars Exploration Scout.[8–11]

Aerodynamic-Structural Optimization Methodology

The importance of interactions between the aerodynamics and the structures is a crucial element in the multi-disciplinary design environment that realizes a flight vehicle. Our initial attempts in addressing this issue used the RANS equations to model the fluid and a simplified structural model that determined a fully stressed structural layout for the given aerodynamic loads. This approach was further refined to include a detailed finite element model for the wing consisting of skins, spars and ribs. Using FEAP, a finite element analysis package developed by Robert Taylor at University of California at Berkeley, iterative aero-elastic simulations were performed to realize the static deflected shape.

The optimal structural layout is now determined using the idea of topology optimization[12] that has its basis in optimal control of the equations of static, linear elasticity. Typically, an engineer is interested in the design of a structure with minimum weight while satisfying the compliance conditions with respect to the external loads, while also satisfying the constraints on maximum allowable stress. This problem has been widely studied using a discrete adjoint formulation in conjunction with the use of a regularizing method that transforms the originally ill-conditioned integer optimization problem to one of continuous optimization. Thus the optimization problem can be written using a penalty function approach as

$$I(\sigma, \rho) = \int_D \rho dV + \alpha \int_D (\sigma(x^s) - \sigma_{max})^2 \delta(x^s - x) dV,$$

where ρ is the density at each point in the structural domain (D), α is the penalty parameter on the violation of the stress constraints, σ is the stress field in the domain, σ_{max} is the maximum allowable stress, δ is the kronecker delta function that enables the inclusion of a domain integral in the objective function for the pointwise stress constraints.

The constraint equations are the governing equations for linear elasticity

$$\frac{\partial \sigma_{ij}(u)}{\partial x_j} + f_j = 0,$$

where f_j are the combined external and internal loads on the structure and u is the displacement field. The optimization problem can now be posed as follows,

$$\begin{aligned} & \min_{\rho} I(\sigma, \rho) \\ s.t. \quad & \sigma_{ij,j} + f_j = 0 \\ and \quad & 0 \leq \rho \leq 1. \end{aligned} \tag{7}$$

Note that constraint equation is similar in form to the viscous operator for the Navier-Stokes equation. Proceeding in a manner similar to shape optimization for flow problems, we write the variation in the cost function as

$$\delta I = \frac{\partial I}{\partial \sigma} \delta\sigma(u) + \frac{\partial I}{\partial \rho} \delta\rho.$$

The variational form the constraint equations, $R(\sigma, \rho) = 0$, for an arbitrary test function ϕ, can be written as

$$\int_D \phi \delta R(\sigma, \rho) = 0,$$

where,

$$\delta R = \frac{\partial R}{\partial \sigma}\delta\sigma + \frac{\partial R}{\partial \rho}\delta\rho.$$

Here the dependence of the constraint equation on the control variable, ρ, is through the definition of the Young's modulus,

$$E(\rho) = \left(\frac{\rho}{\rho_0}\right)^{\beta} E(\rho_0).$$

This regularization enables ρ to vary smoothly between 0 and 1. Integration of the terms in the variational form of the constraint that contain terms corresponding to the variation in the stresses by parts can be written as

$$\int_B \phi\delta\sigma dB - \int_D \frac{\partial\phi}{\partial x_i}\sigma_{ij} dV.$$

The first term represents an integral over the boundary of the domain and the test function on the boundary can be chosen to cancel the term in the variation of the cost function that depends on the variation in the stresses. The second term can be integrated by parts again after noting that

$$\sigma_{ij} = E(\rho)\frac{\partial u_i}{\partial x_j}$$

$$\int_B \frac{\partial\phi}{\partial x} E\delta u_i - \int_D \frac{\partial}{\partial x_i} E \frac{\partial\phi}{\partial x_j},$$

where the first term is identically equal to zero as the displacements are either prescribed as boundary conditions or as a compliance condition. The second term along with the boundary conditions on the test function along the boundary is the adjoint equation. It has a form similar to the constraint equation (as is well-known that equations of linear elasticity are self-adjoint) and can be solved using the FE procedure used to obtain the displacement field. Then the cost variation reduces to

$$\int_D \left(1 - \phi^T \frac{\partial}{\partial x_i}\frac{\partial E}{\partial \rho}\frac{\partial u_i}{\partial x_j}\right) \ \delta\rho \ dV,$$

where the bracketed expression can now be recognised as the gradient. Hence, we can use a similar adjoint approach to determine the sensitivities of a given performance measure with respect to the shape variables and the structural layout to provide a unified approach to concurrently optimize the aerodynamic and structural control variables.

We redesign both wing section and planform to minimize the cost function that is representative of performance metrics in practical design environments. We take convex combinations of the aerodynamic (drag) and structural performance (weight) measures to form a combined metric which can be written as

$$I = \alpha_1 C_D + \alpha_2 \frac{1}{2}\int_{\mathcal{B}} (p - p_d)^2 dS + \alpha_3 C_W. \tag{8}$$

This form of the metric enables the designer to evaluate the trade-offs between improvements in aerodynamic and structural performance. Furthermore, by varying the α-vector, pareto fronts can be established. The aerodynamic-structural optimization procedure is schematically depicted in Figure 3 and the structural optimization is embedded as an inner loop in the overall design process.

The wing section is modeled by surface mesh points and the wing planform is modeled by several global design variables, such as chord at various locations, span, sweepback, and wing thickness ratio.[13] The structural model can be as detailed as desired, but presently includes the main wing box, ribs and spars (Figure 4). The calculations allow for optimization of both the sizes and layout of the structural elements under the wing loads, and changes in the aerodynamic flow due to the wing deflection. A recent aerodynamic-structural redesign of a Boeing 747 wing using this approach, but with a lower-fidelity structural model, reduced the wing drag coefficient from $C_D = 0.0137$ to $C_D = 0.0114$ in 20 design cycles with the wing lift coefficient fixed at $C_L = 0.45$, while simulataneously reducing the calculated wing weight by 1211 pounds.[14]

Results

Seven wing-body configurations were studied with varying sweep angles (35°, 30°, 25°, 20°, 15°, 10°, 5°). The Mach number was systematically reduced from 0.85 for the highest sweep to 0.79 for the lowest sweep wing, while the lift coefficient was simultaneously increased to maintain MC_L roughly constant. Initial aerodynamic shape optimizations were performed on these configurations, subject to the constraint that thickness could not be reduced anywhere on the wing. The results of this study are summarized in Table 2. These optimizations show that the ML/D of the different configurations are all within 1.8% of the maximum value, suggesting a relatively flat design space for aerodynamic performance. Moreover, taking $\sqrt{M}L/D$ as a better approximation to range factor, this trend yields up to a 4% improvement favoring the lower swept wings. At the very least, these results show promise that reduced wing-sweep designs are possible for efficient transonic cruise.

To illustrate the effectiveness of the aerodynamic shape optimizations performed herein, Figure 5 provides the evolution of the pressure distributions for the $\Lambda = 10°$ sweep wing. Pressure distributions of the seed wing are depicted by the *design-00* dashed-line curves. Also included are intermediate states for design cycles 10, 20, and 35. Pressure distributions of the final design are given by the solid-line curves of *design-50*. The seed wing exhibits very strong shocks over most of its span. During the evolution of this optimization, the shock system is monotonically reduced in strength, with the final design comprising only very weak shock waves. Note that the drag of the seed wing is 207.3 counts and that the drag of the final design is 157.3 counts; hence, the optimization reduced the wing drag by 50 counts, about 25% in this case. This represents a substantial enhancement in aerodynamic performance which would most likely never be realized by a cut-and-try approach.

The wings obtained from the aerodynamic shape optimizations were then used in an aerodynamic-structural optimization procedure; this coupled method also allows for modest planform variations within limits set by the feasability of morphing the mesh. The procedure is outlined in Figure 3 and is a two-stage process. Following an aero-elastic simulation and an aerodynamic adjoint calculation, the structural elements are redesigned while holding the aerodynamic loads fixed. Once a structure with minimum weight is obtained that satisfies the stress constraints, the gradients for the airfoil points and the planform variables are determined to find the design that leads to an aerodynamic and structural performance improvement. With this new design, the sequence of aerodynamic-structural simulations and aerodynamic and structural adjoint calculations are repeated until a local minimum is determined.

The results of the aerodynamic-structural optimizations are summarized in Table 3. A similar behavior is observed for the different optimized designs. The aerodynamic performance is approximately the same and the structural weight is also roughly constant, suggesting that the aerodynamic-structural design space is also relatively flat. The planform variables of sweep and span in particular, reveal interesting trends. The optimizer tended to slightly increase the sweep across the various configurations, while the span was slightly increased for the higher sweepback wings and slightly decreased for the lower swept-back cases. The aerodynamic-structural optimizations permit changes in the wing thickness, and in fact the thickness of the outboard wing was slightly reduced at the lower sweep angles, yielding a small reduction in shock drag which contributes to the trend of an increase in the range factor $\sqrt{M}L/D$ with reduced sweep. Similar to the pure aerodynamic optimizations, there is about a 4% improvement in range factor for the lowest swept wing. The actual wing sections of the optimized 35° and 10° swept wings are displayed in Figures 13-14. Figure 13 shows that the primary difference between the aerodynamic-structural and pure aerodynamic optimizations for $\Lambda = 35°$ is in the thickness of the outboard airfoil sections near the critical station. Figure 14 illustrates that this trend for the $\Lambda = 10°$ case is more exaggerated. Just as interesting, varying the sweep for the pure aerodynamic optimizations has a dramatic effect on the airfoil camber distribution, as seen in Figure 15.

In the studies summarized by Tables 2-3 the lift coefficient was varied to maintain a roughtly constant MC_L, with the consequence that variations of ML/D are dictated by the value of C_D. In fact the optimum cruising lift coefficient may vary with Mach number in a different manner. To address this question, we selected the $\Lambda = [10°,\ 35°]$ wings for further analysis. As can be seen from Tables 4-5, the lift-to-drag ratios (L/D) of both wings show an increasing trend as the lift coefficient is further increased. However, it is doubtful whether a practical design could operate at such high lift coefficients for a variety of reasons. First, these results are for single-point optimizations, and when the design point is too extreme it typically leads to a rapid degradation away from the design point. Second, the wing must be able to support a $1.3g$ turn without experiencing buffet, and this sets a limit on the usable design lift coefficient. Third, very high lift coefficients may require an excessively high cruising altitude beyond the capability of the engines, or else require a decrease in wing area with a consequent decrease in fuel volume.

Conclusions

The results of this study suggest that it may be possible to design wings for commercial transport aircraft with low sweep without incurring either aerodynamic or structural performance degradations. The relatively flat design space, both in the aerodynamic and aerodynamic-structural domains, also provides robustness to the designs. On shorter range routes, say less than 1000 miles, the time savings of increasing the Mach number beyond 0.8 are negligible. The present design studies provide an indication that in this case it might be better to use a wing with reduced sweep, or a completely unswept wing, particularily when one takes account of the take-off, climb, descent, and landing segments of the flight profile. On very long range flights the benefits of a reducton in flight time favor a swept wing with a higher cruising Mach number, even if there is no benefit in range efficiency. It may be desirable to maintain commonality of the airframes for the short and long range missions, which would favor the choice of a swept wing. Both the Boeing 737 and the Airbus 320 cruise at Mach numbers below 0.8. If the designers of these aircraft had had access to the current supercritical wing and multi-disciplinary optimization technology, it seems possible that they might have elected to use wings with significantly less sweepback.

While the outcome of the present investigations have unvieled some interesting trends associated with the $M\Lambda T$ design space, the authors feel that more studies should be conducted in this regard to better quantify the magnitude of the potential benefits. For example, it would be beneficial to conduct similar exercises in collaboration with a larger and more diverse team of experts in a realistic airplane design environment. Nonetheless, with the existing aerodynamic shape optimization software, the possibility of enhancing the current knowledge base of the $M\Lambda T$ relationships now appears to be quite feasable.

Acknowledgements

The aerodynamic optimization technologies utilized herein have greatly benefited from the long-term and continuing support of the AFOSR Computational Mathematics Program directed by Dr. Fariba Fahroo. All computations were performed on the facilities of Intelligent Aerodynamics, including three 12-processor Orions and an HPC Box Cluster comprised of four dual-core CPUs running at 3 GHz. The second author extends his appreciation to The Boeing Company for allowing his participation in this and other similar collaborations.

References

[1]A. Jameson. Computational aerodynamics for aircraft design. *Science*, 245:361–371, 1989.

[2]A. Jameson. Aerodynamic design via control theory. *Journal of Scientific Computing*, 3:233–260, 1988.

[3]A. Jameson. *Optimum Aerodynamic Design Using Control Theory, Computational Fluid Dynamics Review 1995.* Wiley, 1995.

[4]A. Jameson. Efficient aerodynamic shape optimization. *AIAA Paper 2004-4369*, 2004.

[5]J. C. Vassberg and A. Jameson. Aerodynamic Shape Optimization Part 1: Theoretical Background. Lecture Series - Introduction to Optimization and Multidisciplinary Design, von Karman Institute for Fluid Dynamics, Brussels, Belgium, March 2006.

[6]A. Jameson and J. C. Vassberg. Studies of alternative numerical optimization methods applied to the brachistochrone problem. In *CFD Journal, Vol. 9, No. 3*, pages 281–296, Kyoto, Japan, October 2000. Japan Society of CFD.

[7]A. Jameson, L. Martinelli, and J. C. Vassberg. Using computational fluid dynamics for aerodynamics - A critical assessment. *ICAS Paper 2002-1.10.1*, 23rd International Congress of Aeronautical Sciences, Toronto, Canada, September 2002.

[8]A. Jameson and J. C. Vassberg. Computational fluid dynamics for aerodynamic design: Its current and future impact. *AIAA paper 2001-0538*, Reno, NV, January 2001.

[9]J. C. Vassberg and A. Jameson. Aerodynamic shape optimization of a Reno race plane. *Int'l Journal of Vehicle Design*, 28(4):318–338, 2002. Special Issue on: Design Sensitivity and Optimization.

[10]J. C. Vassberg, G. S. Page, R. J. Foch, and A. Jameson. Aerodynamic design and optimization of the Mars airborne remote exploration scout. *AIAA Paper 2004-0401*, 42^{nd} AIAA Aerospace Sciences Meeting and Exhibit, Reno, NV, January 2004.

[11]J. C. Vassberg and A. Jameson. Aerodynamic Shape Optimization Part 2: Sample Applications. Lecture Series - Introduction to Optimization and Multidisciplinary Design, von Karman Institute for Fluid Dynamics, Brussels, Belgium, March 2006.

[12]M. P. Bendsoe and N. Kikuchi. Generating optimal strategies in structural design using a homogenization method. *Computer Methods in Applied Mechanics and Engineering*, 71(2):197–224, November 1988.

[13]K. Leoviriyakit. Wing planform optimization via an adjoint method. *Stanford University Thesis*, February 2006.

[14]A. Jameson, K. Leoviriyakit, and S. Shankaran. Multi-point wing planform optimization using control theory. *AIAA Paper 2007-0764*, 45^{th} AIAA Aerospace Sciences Meeting and Exhibit, Reno, NV, January 2007.

Table 1 *Sweep-Span* **Relationship of Study Wings**

Sweep	*Initial Span* (ft)	*A-S Span* (ft)
35°	192.79	193.76
30°	202.72	203.66
25°	211.25	212.30
20°	218.33	218.81
15°	223.88	224.76
10°	227.88	227.76
5°	230.29	229.54

A-S Span: Aero-Structural Optimized Span

Table 2 Optimum Pure Aerodynamic Performance

Mach	*Sweep*	C_L	C_D	$C_{D.tot}$	ML/D	$\sqrt{M}L/D$
0.85	35°	0.500	153.7	293.7	14.47	15.70
0.84	30°	0.510	151.2	291.2	14.71	16.05
0.83	25°	0.515	151.2	291.2	14.68	16.11
0.82	20°	0.520	151.7	291.7	14.62	16.14
0.81	15°	0.525	152.4	292.4	14.54	16.16
0.80	10°	0.530	152.2	292.2	14.51	16.22
0.79	5°	0.535	152.5	292.5	14.45	16.26

C_D in counts, $C_{D.tot} = C_D + 140\, counts$

Table 3 Optimum Aerodynamic-Structural Performance

Mach	Sweep	C_L	C_D	C_W	Cost	ML/D	$\sqrt{M}L/D$
0.85	35°	0.500	151.7	0.03562	0.01846	14.57	15.80
0.84	30°	0.510	148.7	0.03531	0.01831	14.84	16.19
0.83	25°	0.515	147.6	0.03537	0.01847	14.86	16.31
0.82	20°	0.520	148.2	0.03500	0.01839	14.80	16.34
0.81	15°	0.525	148.7	0.03465	0.01845	14.73	16.37
0.80	10°	0.530	148.6	0.03464	0.01852	14.69	16.43
0.79	5°	0.535	148.9	0.03455	0.01842	14.63	16.46

C_D in counts, $Cost = (\alpha_1 C_D + \alpha_2 C_W)$ maximizes Breguet Range

Table 4 Envelope of Optimized Drag Polars for the 10° **Sweep Wing at Mach 0.80**

C_L	C_D	$C_{D.tot}$	L/D	C_W	ML/D	$\sqrt{M}L/D$
0.5336	151.5	291.5	18.36	0.03464	14.69	16.42
0.5448	154.0	294.0	18.53	0.03466	14.82	16.57
0.5556	157.5	297.5	18.68	0.03461	14.94	16.71
0.5663	161.1	301.1	18.80	0.03456	15.04	16.82
0.5881	168.6	308.6	19.04	0.03452	15.23	17.03

Table 5 Envelope of Optimized Drag Polars for the Baseline 35° Sweep Wing at Mach 0.85

C_L	C_D	$C_{D.tot}$	L/D	C_W	ML/D	$\sqrt{ML/D}$
0.4998	151.4	291.4	17.16	0.03562	14.59	15.82
0.5100	153.3	293.4	17.38	0.03561	14.77	16.02
0.5334	162.2	302.2	17.54	0.03559	14.91	16.17
0.5556	171.9	311.9	17.81	0.03554	15.14	16.42
0.5780	181.2	321.2	17.99	0.03550	15.29	16.59
0.5900	192.9	332.9	17.72	0.03540	15.06	16.34

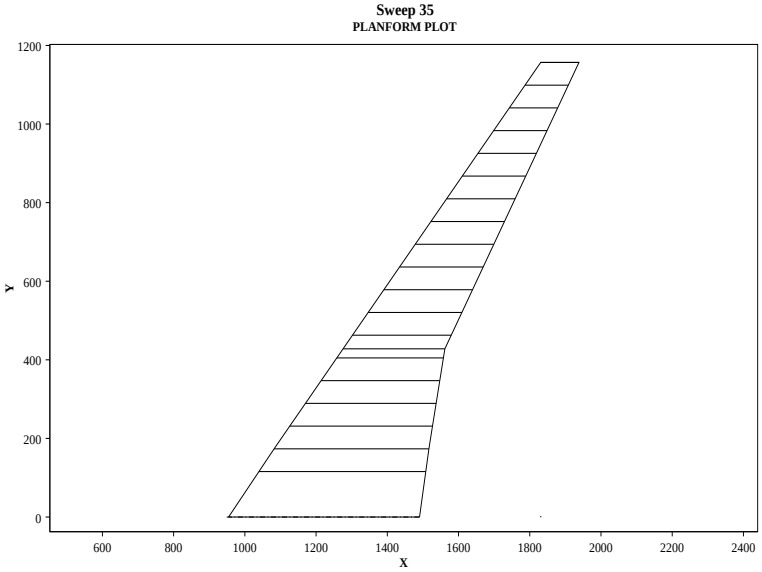

Fig. 1 Planform of Baseline $\Lambda = 35^\circ$ Wing

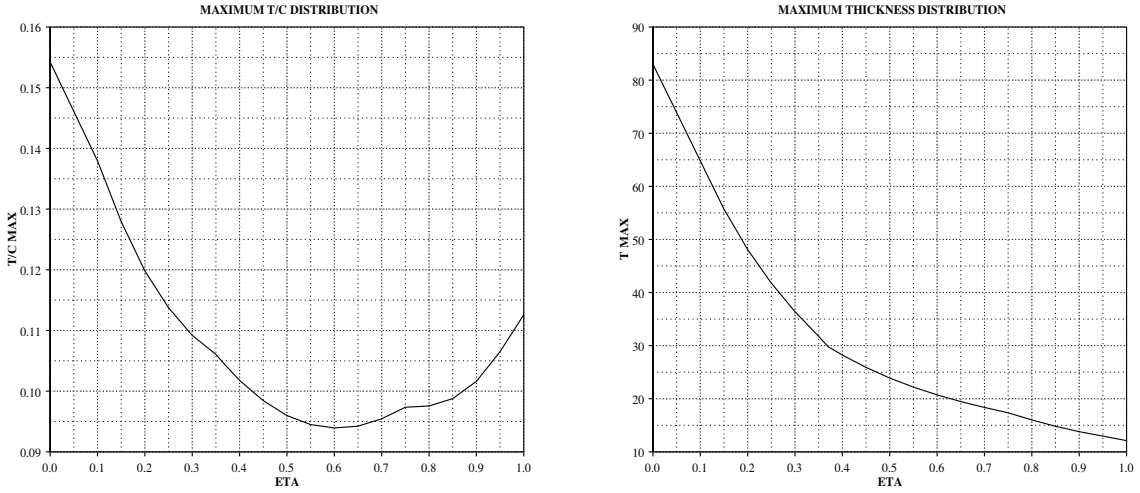

Fig. 2 Nondimensional and Absolute ($in.$) Thickness Distributions of Baseline $\Lambda = 35^\circ$ Wing

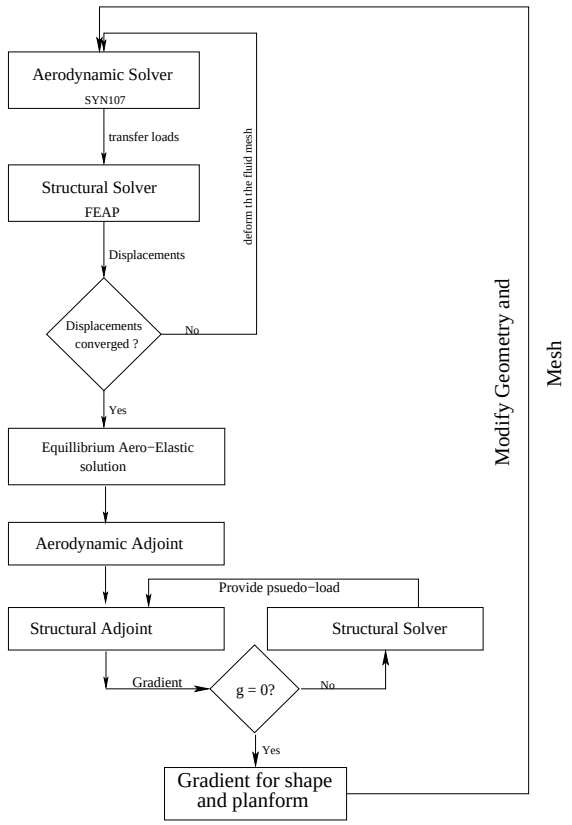

Fig. 3 Overview of Aerodynamic-Structural Design Process

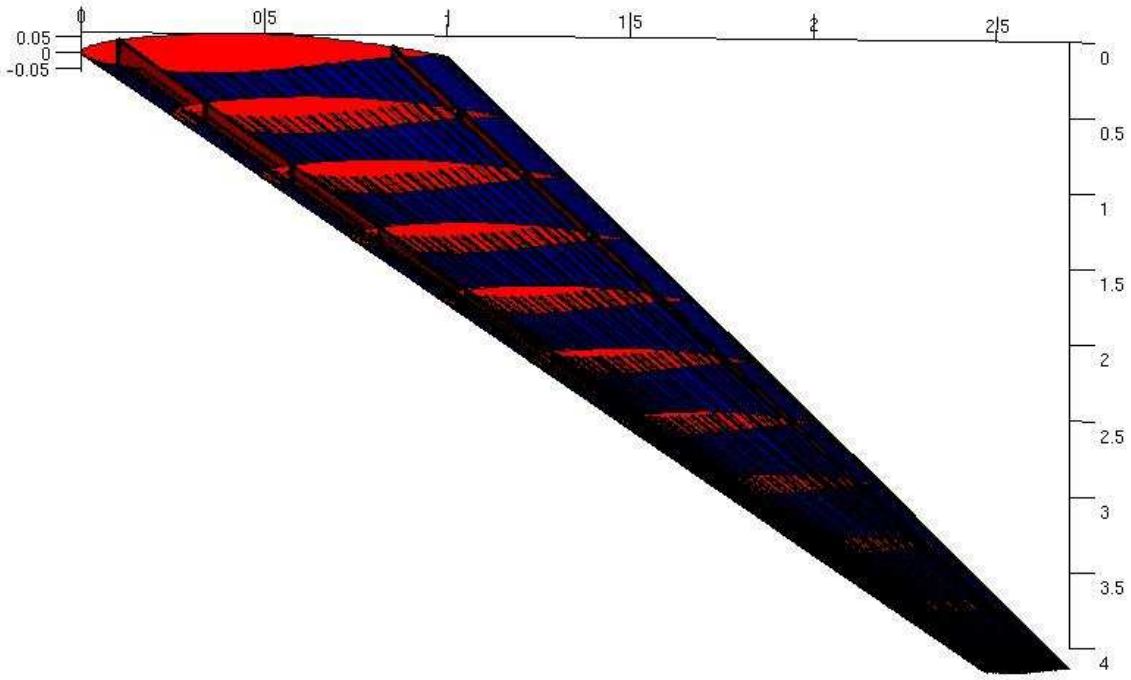

Fig. 4 Cut-Away of Structural Model for Wing, showing Skin, Ribs, Spars and Stiffeners

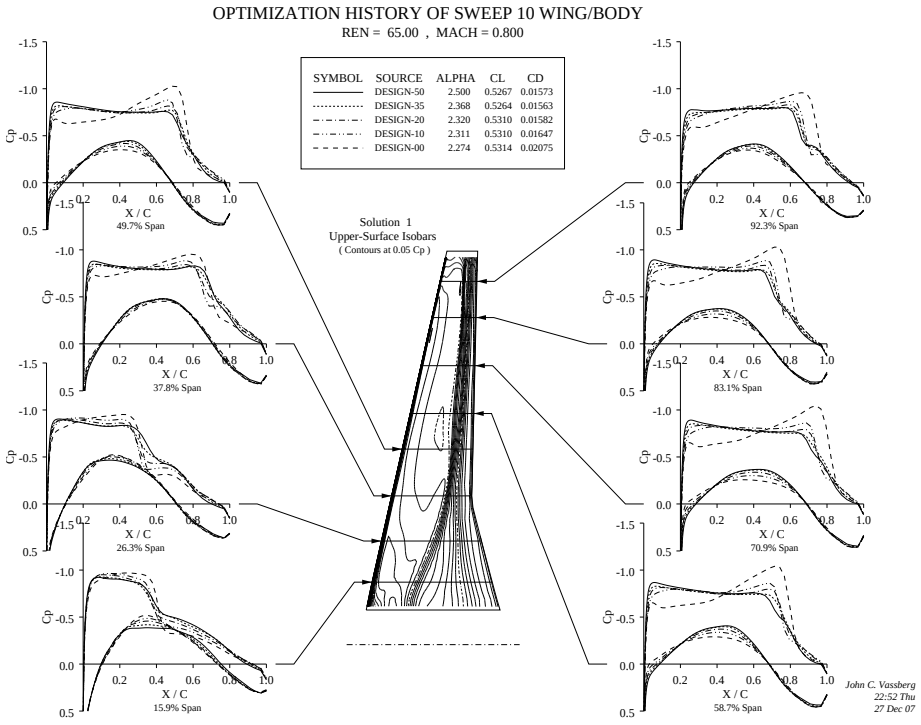

Fig. 5 Evolution of Pressures for the $\Lambda = 10^\circ$ Sweep Wing during Optimization

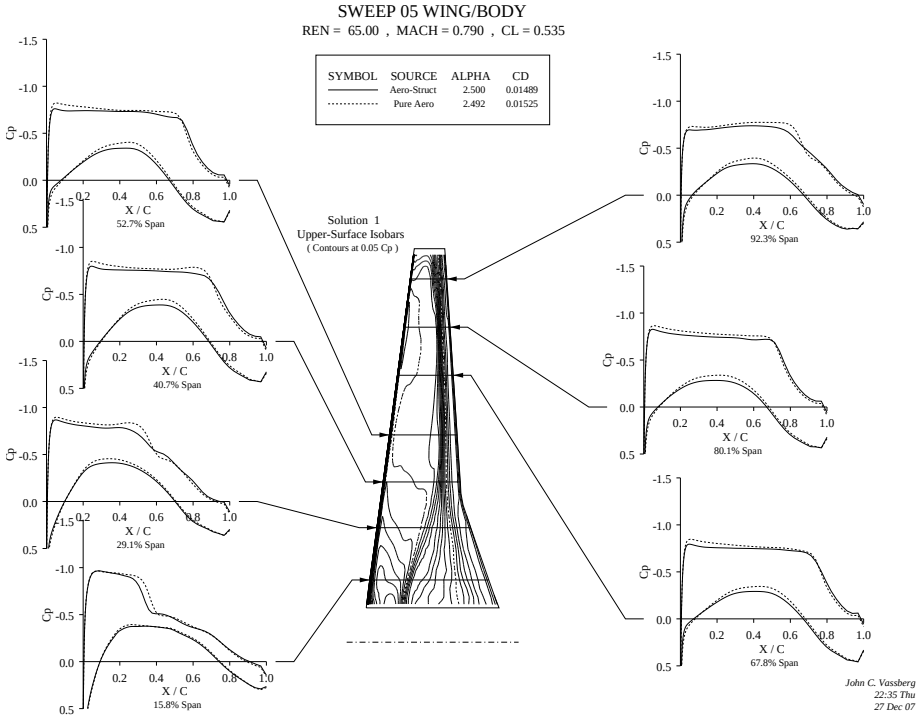

Fig. 6 Optimized Design at Mach 0.79 and $\Lambda = 5^\circ$ Sweep

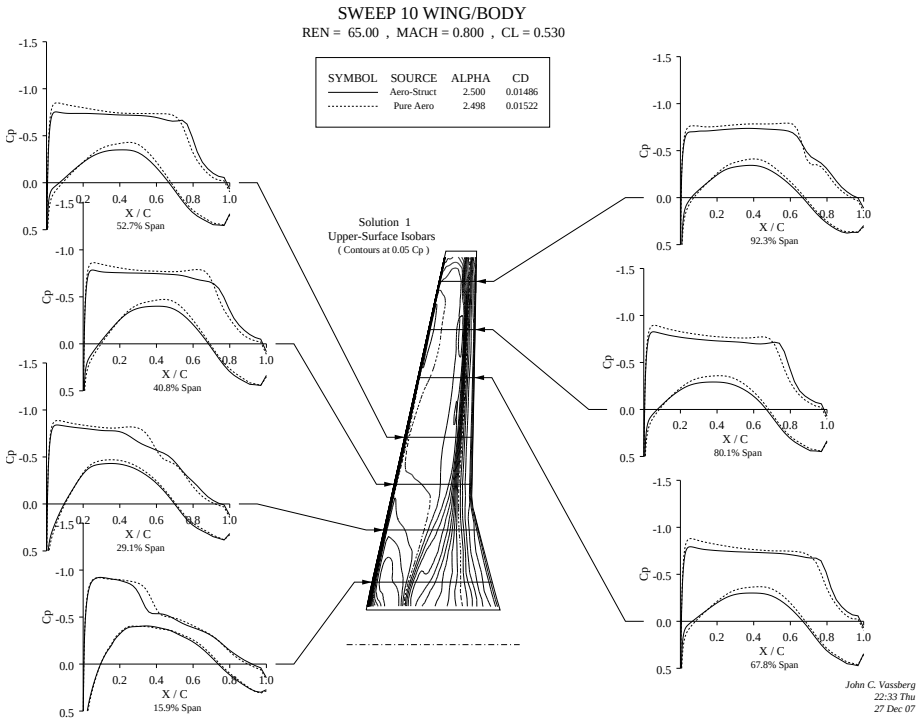

Fig. 7 Optimized Design at Mach 0.80 and $\Lambda = 10^\circ$ Sweep

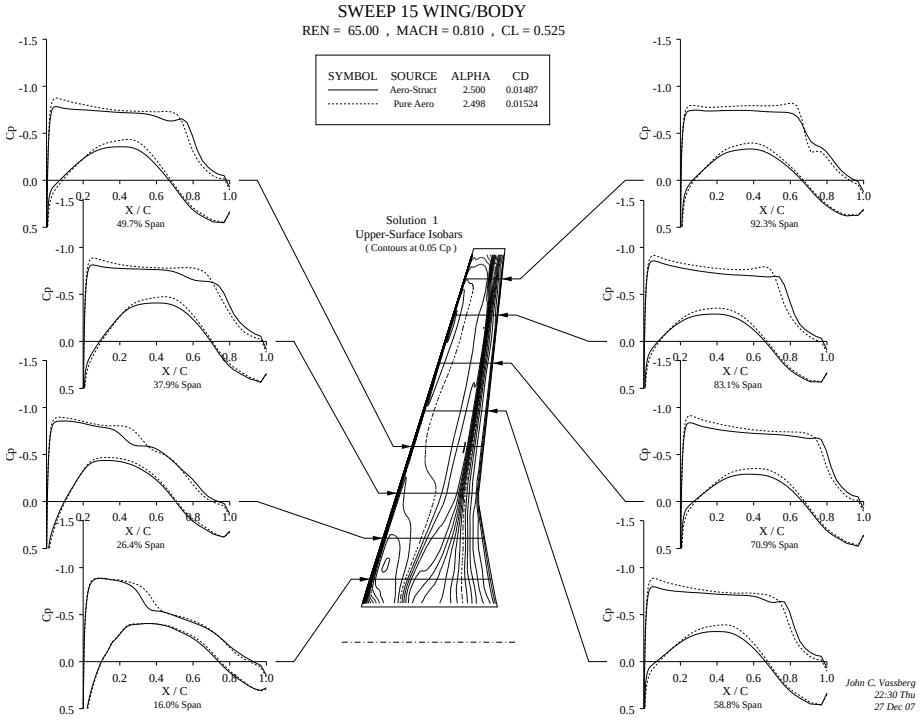

Fig. 8 Optimized Design at Mach 0.81 and $\Lambda = 15^\circ$ Sweep

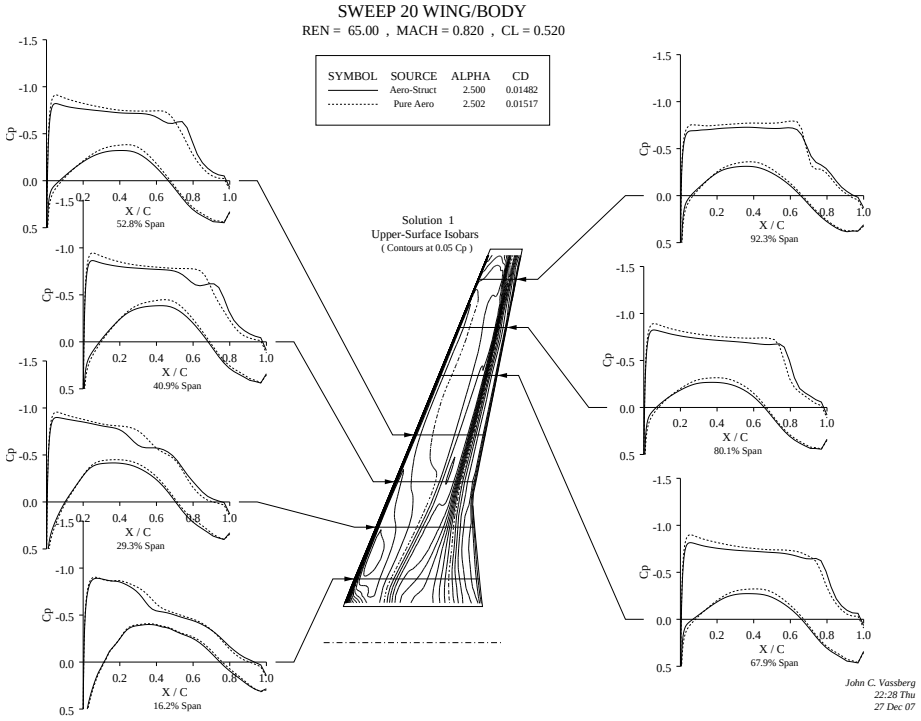

Fig. 9 Optimized Design at Mach 0.82 and $\Lambda = 20^\circ$ Sweep

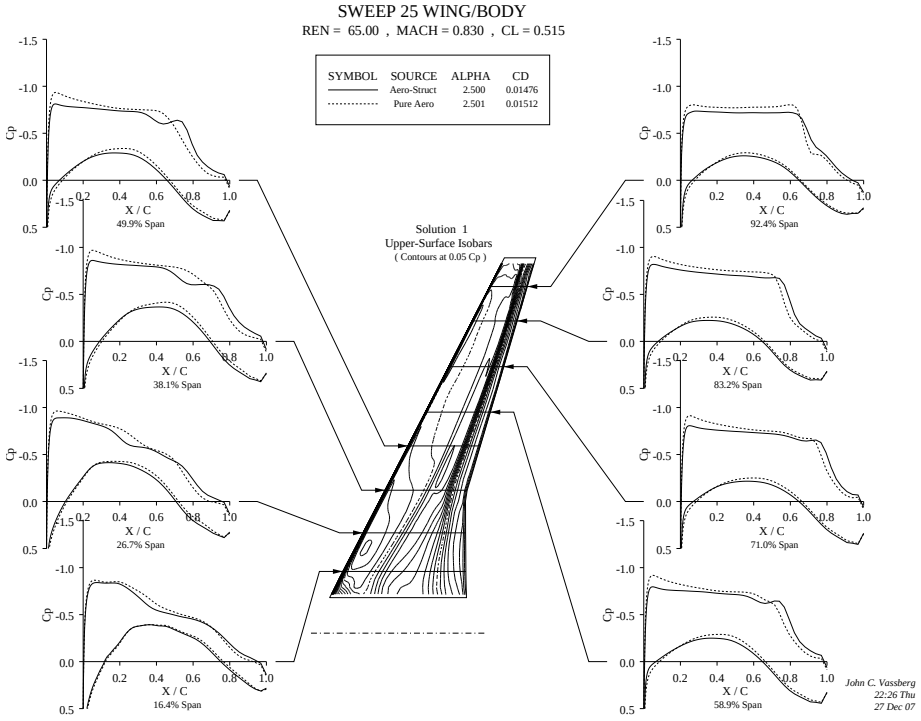

Fig. 10 Optimized Design at Mach 0.83 and $\Lambda = 25^\circ$ Sweep

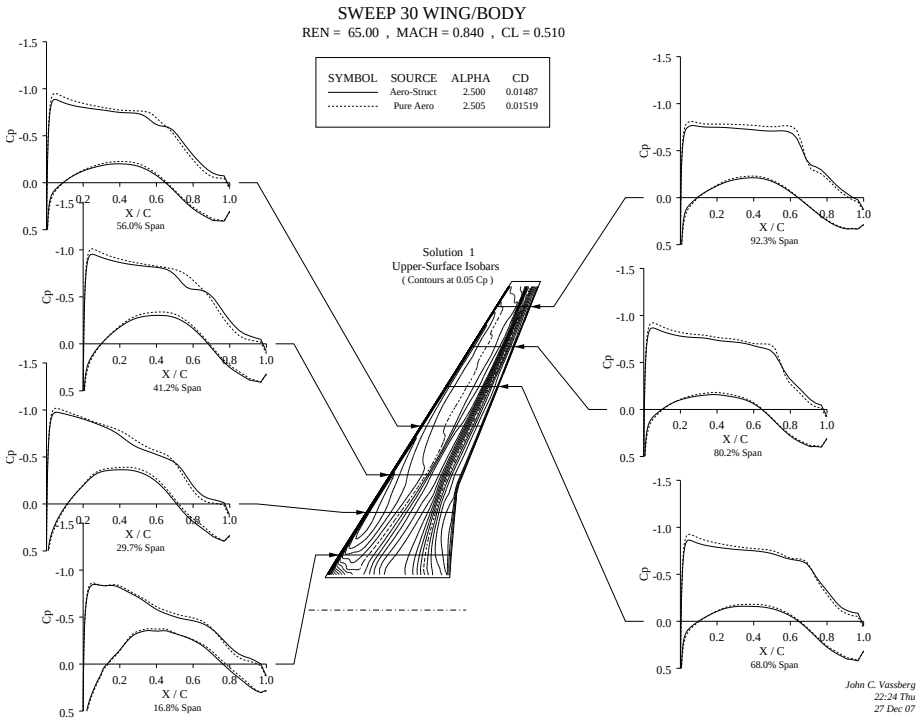

Fig. 11 Optimized Design at Mach 0.84 and $\Lambda = 30^\circ$ Sweep

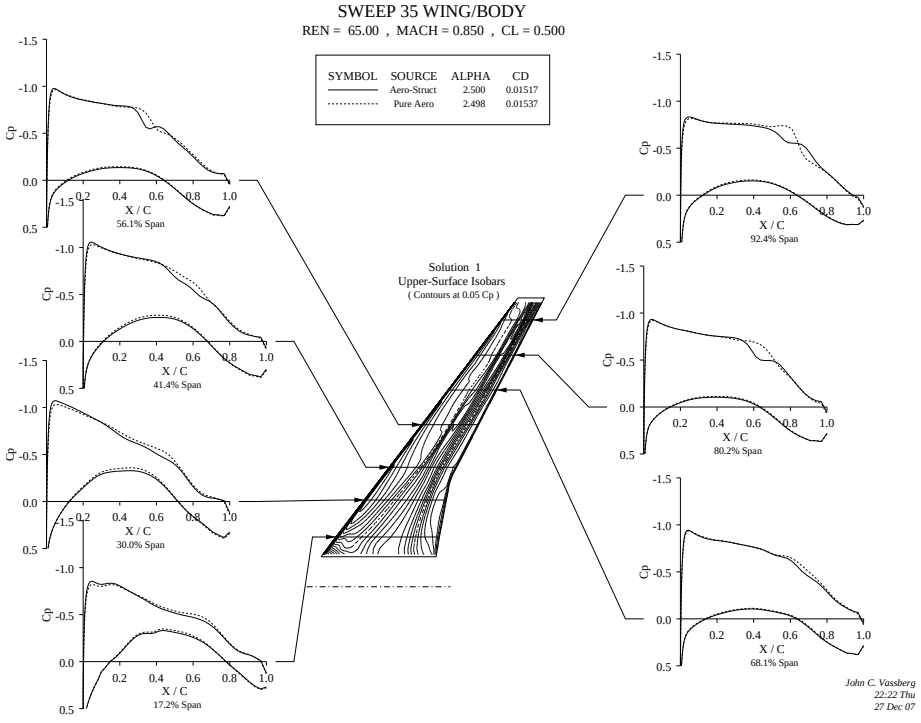

Fig. 12 Optimized Design at Mach 0.85 and $\Lambda = 35^\circ$ Sweep

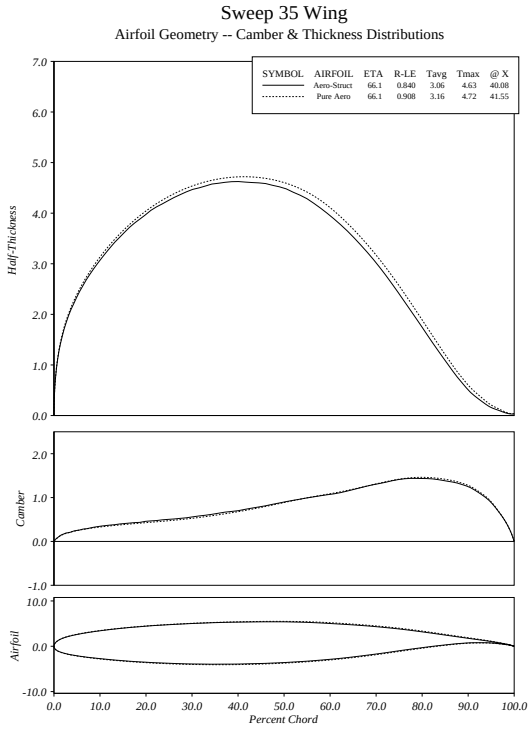

Fig. 13 Airfoil Sections at $\eta = 66\%$ of Optimal $\Lambda = 35^\circ$ Sweep Wings

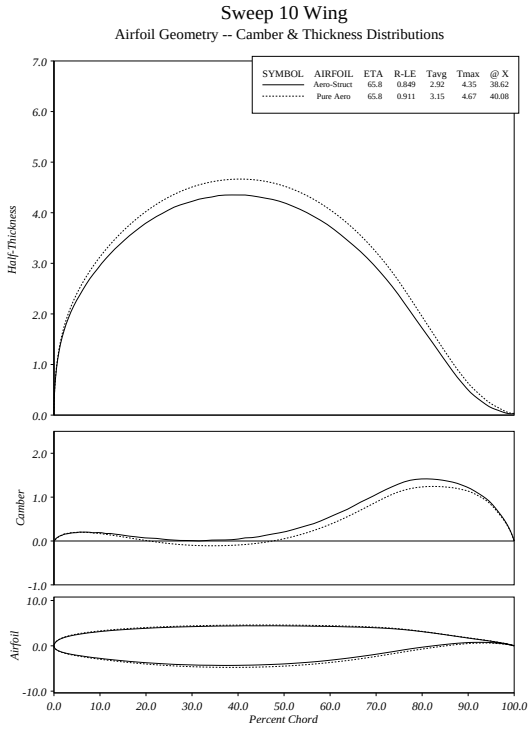

Fig. 14 Airfoil Sections at $\eta = 66\%$ of Optimal $\Lambda = 10^\circ$ Sweep Wings

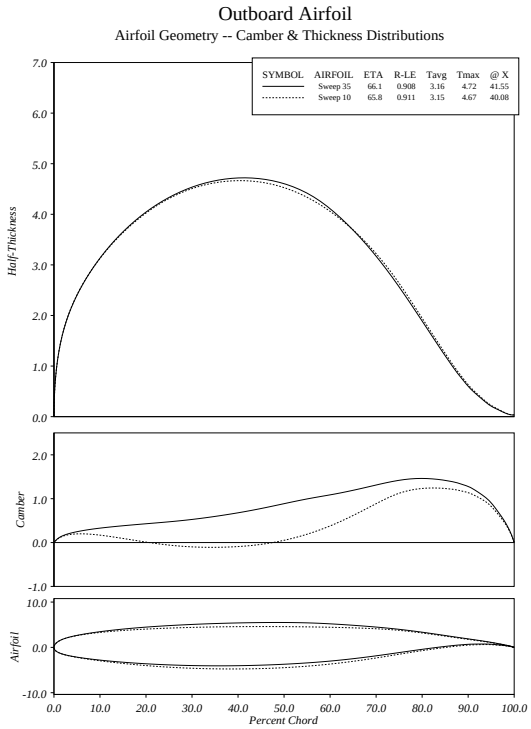

Fig. 15 Airfoil Sections at $\eta = 66\%$ of Optimal $\Lambda = 35^\circ$ and $\Lambda = 10^\circ$ Sweep Wings